Shock Waves
DOI 10.1007/s00193-009-0196-8

ORIGINAL ARTICLE

Height of burst explosions: a comparative study of numerical and experimental results

M. Omang · S. O. Christensen · S. Børve · J. Trulsen

Received: 31 October 2008 / Accepted: 26 February 2009

Abstract In the current work, we use the Constant Volume model and the numerical method, Regularized Smoothed Particle Hydrodynamics (RSPH) to study propagation and reflection of blast waves from detonations of the high explosives C-4 and TNT. The results from simulations of free-field TNT explosions are compared to previously published data, and good agreement is found. Measurements from height of burst tests performed by the Norwegian Defence Estates Agency are used to compare against numerical simulations. The results for shock time of arrival and the pressure levels are well represented by the numerical results. The results are also found to be in good agreement with results from a commercially available code. The effect of allowing different ratios of specific heat capacities in the explosive products are studied. We also evaluate the effect of changing the charge shape and height of burst on the triple point trajectory.

Keywords Blast waves · RSPH · Height of burst

PACS 47.40.-x · 82.40.Fp

Communicated by C. Needham.

M. Omang · J. Trulsen
Institute of Theoretical Astrophysics, University of Oslo,
Postbox 1029, Blindern, 0315 Oslo, Norway

M. Omang (✉) · S. O. Christensen
Norwegian Defence Estates Agency,
Postbox 405, Sentrum, 0103 Oslo, Norway
e-mail: momang@astro.uio.no

S. Børve
Norwegian Defence Research Establishment,
Postbox 25, 2027 Kjeller, Norway

1 Introduction

In the period during and after the Second World War, many experiments were done to investigate air blast, and the effect of detonations of high explosives. There were two main categories, free-field tests and surface explosions. Free-field tests were considered the most ideal, since they were unaffected by reflecting surfaces, whereas in the case of surface bursts, the amounts of energy absorbed into the ground were much more difficult to determine. In most of the empirical data published, pressure sensors were used to measure the maximum overpressure and the shock time of arrival. If the pressure sensors were positioned on a row, average shock velocity could also be determined. The effect of the negative phase was not considered important, and therefore little effort were put in measuring the overall pressure–time history. Due to lack of suitable instrumentation, density and temperature measurements hardly exist [1].

In more recent experiments, pressure gauges are still the most used instrumentation for air blast measurements, although photographic and optical techniques are now more common. An example is the introduction of small tracer-particles, so-called smoke trails, launched into the air right before the blast wave arrives. If the smoke trails are combined with high-speed video filming, the particle velocities and density can be computed [4,5]. There are also reports on full-scale Schlieren imaging of shock waves [13], although for practical reasons, these optical techniques still seem best suited for visualization and high-precision laboratory work.

We use empirical data from two different databases in the present paper [6,7], in addition to results from our own experiments. The empirical data includes maximum overpressure, shock time of arrival, positive phase duration, and pressure impulse. Although the data also illustrates the uncertainty

Published online: 24 March 2009

in experimentally measured data, they are well suited for comparison with numerically computed results.

The explosion is handled with a rather simple explosive model called the Constant Volume Model (CVM), in which a set of assumptions allow numerical computations to be achieved with a single-phase model. The CVM model is implemented into the numerical method Regularized Smoothed Particle Hydrodynamics (RSPH) and a commercially available method, Chinook.

We explore the capabilities of RSPH to handle detonations and propagation of blast waves. In the course of this work, we wish to exploit the formulation for spherical and axial symmetries in RSPH, which has been previously tested against numerical benchmark tests such as the Sod problem, Noh test, and the Sedov test [9,10], as well as more complex problems such as a the expansion and reflection of coaxial and torus-shaped shocks [11]. The main goal of the present work is to demonstrate that the CVM model together with the RSPH method produces high precision results as compared to experimental results and also results from a different numerical method.

In the next section, we give a brief introduction to our numerical method, followed by a description of the high explosive model in Sect. 3. The model is tested on simulations of free-field explosions, and the data are compared to experimental results. In Sect. 4, we take a closer look at a series of tests performed with high explosives at various heights above ground, so-called Height of Burst (HOB) tests. The results from simulations of these tests are compared to results obtained from pressure sensors. The effects of changing the charge shape and HOB are discussed in further detail. A parameter study of different ratio of specific heat capacities in the high explosive products is performed. In Sect. 5, the results are summarized and discussed.

2 A brief description of the numerical method

In the current work, we will mainly use the numerical method Regularized Smoothed Particle Hydrodynamics (RSPH), to study blast waves from explosive charges. For comparison purposes, we also include results from simulations with a commercially available numerical code. For further details the reader is referred to Chinook.[1] Since a detailed description of RSPH can be found elsewhere [2,3], we will only give a short description here.

SPH is a Lagrangian particle method [8], where particles rather than grids are used to describe a continuous fluid flow. The particles are given properties of the gas, such as position, mass, density, pressure, velocity, and energy. The particles are also given a characteristic size, called the smoothing length. The evolution of the hydrodynamic properties of the individual particles are determined from their interactions with neighbouring particles. A weight function, called the kernel function, determines the contribution from each neighbouring particle, dependent on their inter-particle distance. Defining a kernel function with finite support, or finite width, means that the number of interacting particles is reduced.

Since the particles move with the flow, the interparticle distances change continuously, and consequently there is a natural adaptivity in the method. Additionally, RSPH allows for particles with different smoothing lengths in the computational domain. Different regions are given different smoothing lengths, but with the restriction that there is only a factor of two difference in smoothing lengths for neighbouring particles. Additionally, the resolution is optimized by a particle regularization process applied at regular time intervals. The new particle population is distributed in a regular lattice, with particle properties determined from the current particle distribution. The resolution in the new particle set, in the form of a smoothing length profile, is based on the properties of the current particle set.

In the present work, we assume no symmetry breaking instabilities to be important in the system, such that any initial spherical or axial symmetry is retained. With such symmetry assumptions 3D simulations may be computed in either 1D or 2D, respectively, thereby saving computational time and cost. A thorough description of the deduction of the equations of motion for a given symmetry through fundamental SPH interpolation theory, is given in [9,10]. Our description differs from previous descriptions by two important features. First of all, the kernel functions are developed with their boundary conditions incorporated in the description, and secondly, the equations of motion are developed with new kernel functions that do not introduce singularities at the origin or the symmetry axis.

3 High explosives modelling

In the current work, we use the Constant Volume Model (CVM) to simulate the detonation of the High Explosives (HE). The CVM is based on the assumption that the transition in the explosive from solid to gas phase essentially takes place instantaneously within a fixed volume. The process is assumed to take place without loss of energy, and we also neglect the effect of after-burning of rest product. The simulations are therefore started with the initial gas products from the detonation as a dense hot "balloon" in its original volume. The CVM allows for the assumption of a single-phase computation using a constant ratio of specific heat capacities, for instance ($\gamma = 1.4$), and the ideal gas equation of state.

[1] Martec Limited, 1888 Brunswick Street, Suite 400, Halifax, Nova Scotia B3J 3J8, Canada: Chinook Manual.

Table 1 HE data

Shape	Charge weight (kg)	HOB (m)	HE	Density (kg/m^3)	Energy (MJ/kg)
Spherical	1.0	Free-field	TNT	1,630	4.26
Hemi-spherical	1.0	Surface burst	TNT	1,630	4.26
Spherical	2.95	1.0	C-4	1,475	5.62
Spherical	2.95	2.0	C-4	1,475	5.62
Cylindrical	2.95	1.0 (bottom)	C-4	1,475	5.26

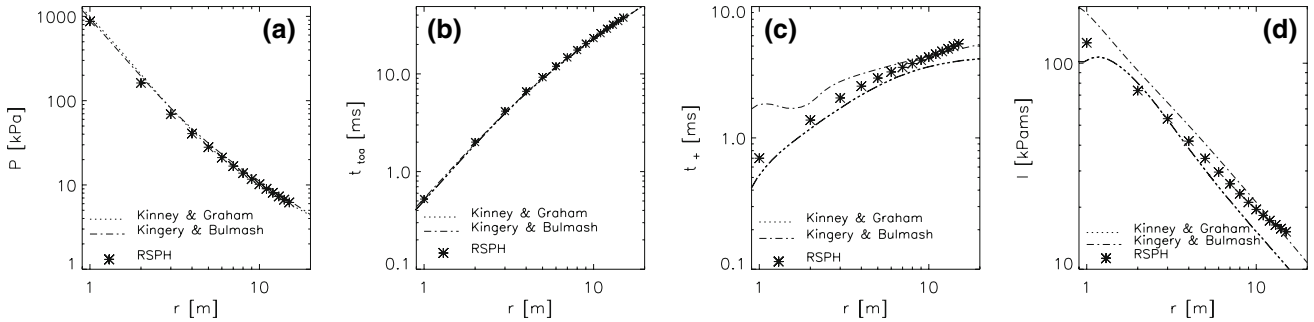

Fig. 1 **a** Maximum overpressure, **b** shock time of arrival, **c** positive phase duration, and **d** pressure impulse for a 1 kg free-field TNT charge. RSPH results are illustrated with *star* symbols, *dashed lines* and *dashed-dotted lines* represent results from two different empirical databases

3.1 Free-field detonation of 1 kg TNT

In order to test the accuracy of the CVM we look at a well documented test case of a 1 kg spherical charge of TNT. The charge is detonated in free-field. For a perfect spherically symmetric detonation, spherical symmetry can be assumed in our computations. The technical data for the HE are given in Table 1, first row. In Fig. 1a, the overpressure P is plotted as a function of distance from the charge center. The RSPH results are illustrated with star symbols. The results are compared to data from two different empirical databases [6,7]. The agreement with the empirical data is clearly good, as the data are plotted nearly on top of each other. Good agreement with empirical data is also observed for the shock time of arrival t_{toa}, as illustrated in Fig. 1b. Again the different curves are hard to distinguish from each other. For the positive phase duration t_+, which is measured from shock time of arrival until the pressure dips below atmospheric pressure, the discrepancy between the two empirical data sets is worth noticing. The RSPH results are largely found to lie within the range spanned by the two empirical data sets. This trend is also observed for the pressure impulse I, computed from the area underneath the overpressure part of the pressure curve,

$$I = \int_{t_{\text{toa}}}^{t_+} P \, \mathrm{d}t. \tag{1}$$

The discrepancy between the two empirical data sets is significant, while the numerically computed data points are again found in the range between the two empirical curves for most distances. Towards the larger distances the slope of the empirical and numerical data differs slightly for both positive duration and impulse. In the numerical simulations we assume an ideal detonation with no afterburning of rest products. The effect of this process would not be observable in peak pressure and time of arrival plots, but may explain the difference in the slopes observed for positive duration and impulse.

3.2 Hemi-spherical detonation of 1 kg TNT

Our second example is a surface burst explosion of a 1 kg charge of TNT. The charge is hemi-spherical, and positioned on the ground. In this case the computations are performed with an axisymmetric code, with the vertical line of symmetry through the center of the charge. The ground is assumed to be a perfect solid boundary, neglecting the effect of cratering or energy absorption into the ground. The technical TNT data are given in Table 1, second row. In Fig. 2, a density color image is plotted for the $r - z$ plane. The color image is based on an interpolation of the particle distribution on to a regular grid, since the particle distribution is continuously changing.

In Fig. 3a, the numerical results plotted with star symbols, are compared to empirical data illustrated with a solid line. The agreement is good, although the overpressure is slightly underpredicted for the larger distances. The agreement of numerical and empirical data for the time of arrival in Fig. 3b indicates that the shock velocity is well represented. When compared to the empirical results, the results

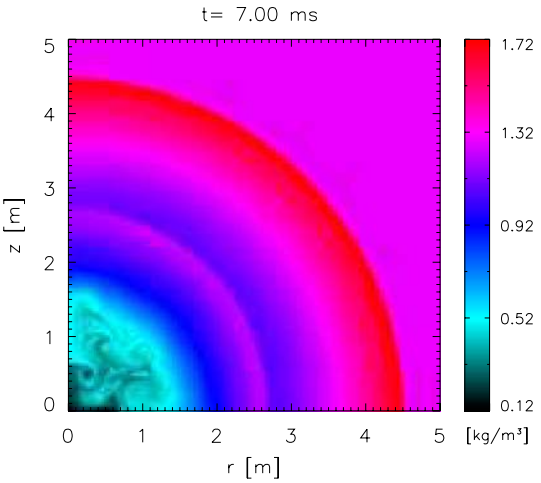

Fig. 2 Density color plot at $t = 7.0$ ms after the detonation of a hemi-spherical 1 kg charge of TNT

for positive phase duration (Fig. 3c) and pressure impulse (Fig. 3d) are less accurately described. As illustrated in the previous section (Fig. 1c, d), these parameters are found to be more demanding to measure correctly.

4 Height of burst explosions (HOB)

In this section, we present results from HOB explosions performed by the Norwegian Defence Estates Agency. The intention is to study the effect of changing the height of burst and shape of charge. Two spherical charges are detonated at HOB = 1 m and HOB = 2 m. Additionally, we study a cylindrical charge detonated at HOB = 1 m. In all three cases, the plastic HE C-4 was applied, and the charge density computed based on the geometry and weight of the thin-walled container in which the HE was filled. A glass container was used for the spherical charges, whereas a plastic container was used in the cylindrical charge case. Technical details from the test series are found in Table 1. The containers were positioned on small wooden platforms, supported by a wooden pole. On the ground, pressure sensors were positioned at increasing distances $r = 4, 5, 6$, and 10 m from ground zero, the charge centre projected onto ground. A picture of the test configuration is presented in Fig. 4.

4.1 Spherical charge, HOB = 2 m

The detonations of the spherical charges are assumed to be symmetric. This allows us to compute the initial phase with our spherically symmetric RSPH formulation. When the shock approaches the ground, the results are mapped onto a larger computational domain, and we change to an axisymmetric formulation. Figure 5 illustrates the density profile in a color plot in the $r - z$ plane at $t = 2.50$ ms after the detonation initiation. The shock has reached the ground and is reflected, and a Mach reflection is about to form, as the reflection point leaves the surface.

Pressure time histories for HOB = 2 m are presented in the left-hand panels of Fig. 6 for increasing distances. The blue lines represent the recorded pressure signals, whereas the black lines show the results of the numerical simulations. The experimentally obtained time zero, when the actual initiation takes place, represents a challenge to measure correctly. In the current experiments, a wire was mounted on the circumference of the charge. When the wire is broken, a signal is measured and used as a time zero for the event. Due to the lack of accuracy in such measurements, the pressure signals presented here are corrected for the time-of-arrival at the first sensor. The correction values are given in Table 2 for the tests presented here. With the timing at the first sensor corrected, the left-hand panels of Fig. 6 illustrate that numerical simulations give a fair description of the shock velocity. Both time of arrival and the pressure levels are well represented by the numerical simulations.

The pressure impulse curves, computed as described in (1), replacing t_+ by $t = 30$ ms, are also plotted in the left-hand panels of Fig. 6 with the same ordinate axis, but this time in units of [kPa ms]. Reasonably good agreement is achieved initially as the shock hits the sensor. Later, the deviations

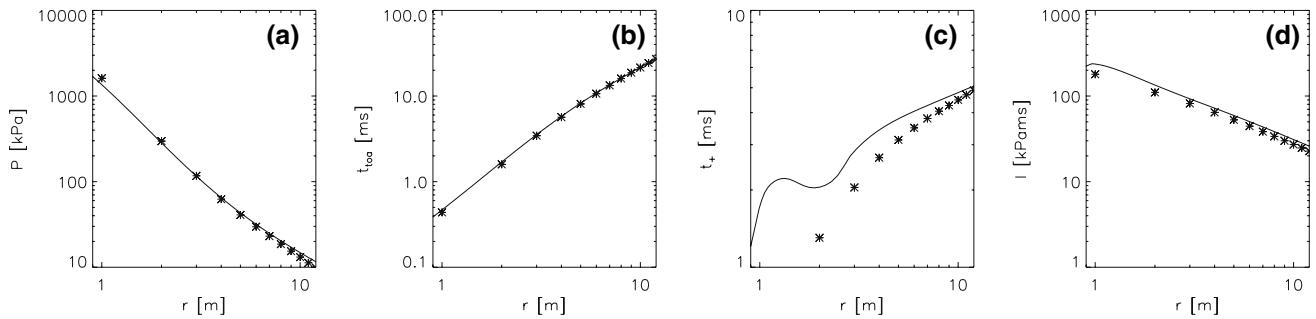

Fig. 3 **a** Maximum overpressure, **b** shock time of arrival, **c** positive phase duration, and **d** pressure impulse for a hemi-spherical 1 kg charge of TNT. The *star* symbols illustrate the RSPH results, whereas the *straight lines* are taken from empirical data of Kingery and Bulmash [6]

Fig. 4 Height of burst test, HOB = 2 m, using the HE C-4. Along the ground 4 sensor platforms are positioned at increasing distances of $d = 4$, 5, 6 and 10 m

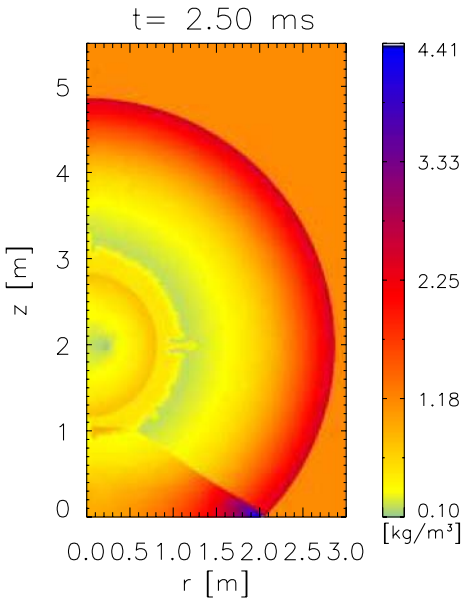

Fig. 5 Density color plot of the $r-z$ plane $t = 2.5$ ms after detonation initiation

between the experimental and simulated data increase. The difference in the two curves, may be due to several reasons. First of all, our HE model does not take afterburning of rest products into account. Secondly, we have made the assumption of a constant ratio of specific heat capacities. Thirdly, the HE was filled into a glass container, which was mounted on a small wooden platform. The effect of the container and the burning of the wooden platform have not been considered.

4.2 Spherical charge, HOB = 1 m

A similar test was conducted by changing the HOB to 1 m. Both charge and the remaining configuration were unaltered. In the right-hand side of Fig. 6, the overpressure and impulse are plotted for increasing distances from the charge. The numerical data are presented with black lines, the empirical data with blue lines. The numerical results have again been corrected for the time of arrival at the first sensor, with the correction values given in Table 2. As for the previous case, we observe that the shock velocity is well captured by the numerical simulations, which is also the case for the pressure levels, for all four sensors.

In order to check the performance of RSPH against a different numerical method, we have also included results from Chinook (see footnote 1), a commercial code developed by Martec Limited. Chinook is an Euler 3D parallel unstructured mesh CFD code with an Harten, Lax and van Leer contact wave (HLLC) approximate Riemann Solver [14]. The current simulations are performed with the same explosive model as RSPH, and the same HE parameters. The results are plotted in the right-hand panels of Fig. 6 with green lines. As for the RSPH data, the results have been corrected for the time of arrival at the first sensor, with correction value given in Table 2. As the figure illustrates, the results produced by the two numerical methods are hardly distinguishable, and the agreement with the empirical velocity and pressure levels are good. When comparing the secondary peak (at about 10 ms in panel a) of the empirical and numerical data, we observed that the fit is less accurate, as both numerical computed peaks are delayed, relative to the empirical one. This effect probably causes the pressure impulse to be less accurate for the remaining signal, after the overpressure curves have dipped below the atmospheric pressure ($P = 0$ kPa) in Fig. 6.

4.3 Cylindrical charge, HOB = 1 m

In our last test, the spherical charge is replaced by a cylindrical charge with a length l to diameter d ratio $l/d = 2$. The HOB in this case is 1 meter, but unlike the spherical tests where HOB is measured to the charge center, the height is measured to the bottom of the charge. The initial phase of the detonation is performed in an axisymmetric code, dynamically adjusting the computational domain to the expanding shock wave. In order to save time, the first $t = 0.3$ ms is computed in a relatively small computational domain.

Figure 7 is a color plot of the cylindrical charge at $t = 0.3$ ms after detonation initiation. The plot clearly illustrates the non-spherical shape of the shock. Between the initial shock and the contact discontinuity (the transition from dark color to lighter blue), a rather complicated pattern is observed. The phenomena observed is a Richtmyer–Meshkov instability, generated due to large density differences in the regions in front of, and behind the shock. The instability pattern consisting of curled spikes are observed to be symmetric across the charge center, $z = 1.108$ m.

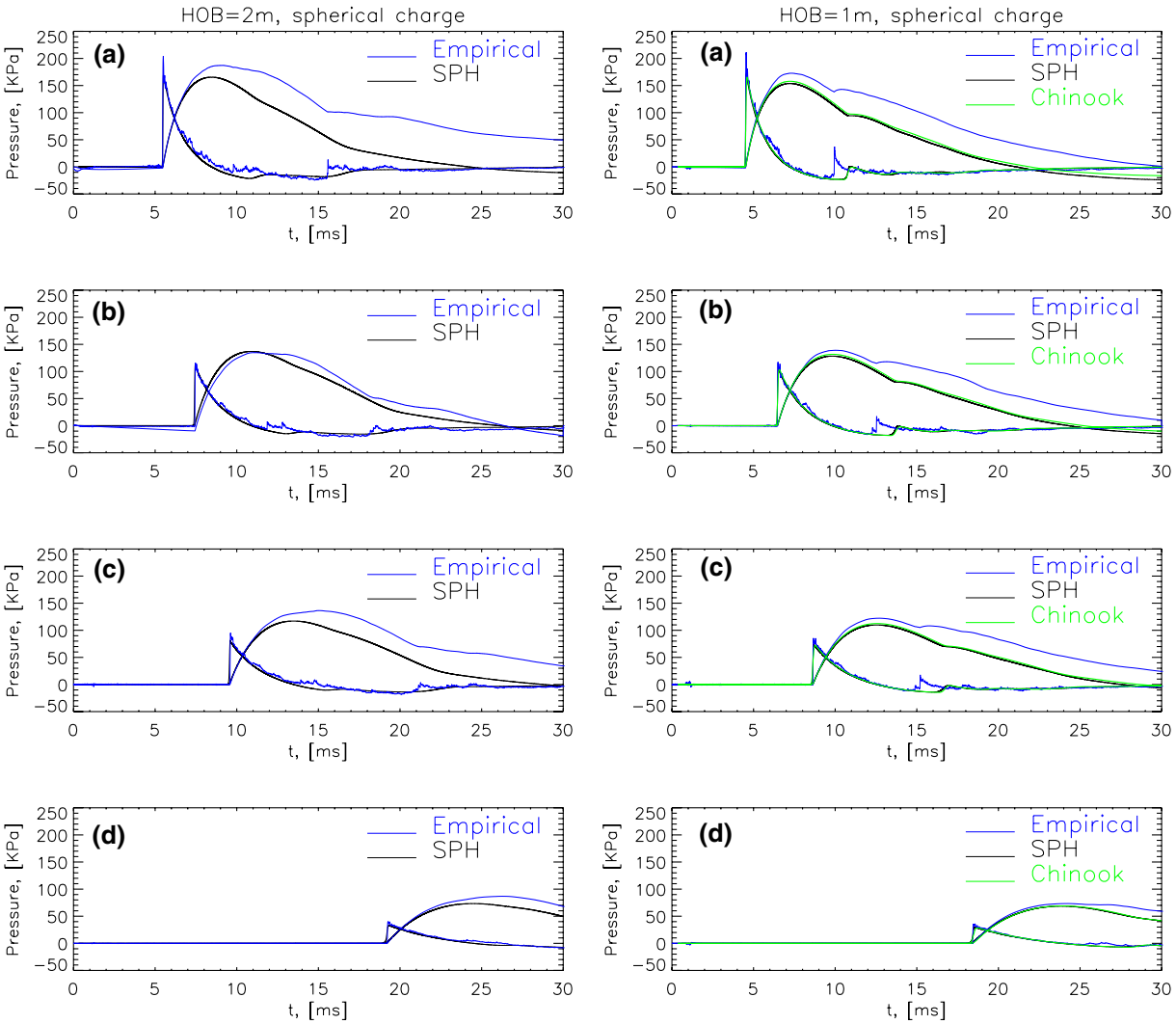

Fig. 6 Overpressure and pressure impulse plotted for charges at HOB = 2 m *left side*, and HOB = 1 m *right side*. The sensors are positioned on the ground at distances of **a** 4 m, **b** 5 m, **c** 6 m, and **d** 10 m

In Fig. 8, the results at the four sensors are presented and compared to the pressure recordings from the test. Also in this case, we find the shock time of arrival to be well represented by the numerical simulations, when compared to the test results. This is also the case for the pressure levels. The impulse is less accurately represented by the numerical results, and may be due to effects not taken into consideration, as discussed in Sect. 4.1. The CVM implies that effects of point of initiation are not taken into account, effects that may be of greater importance for cylindrical charges.

4.4 The effect of introducing γ as a particle property

In the results presented so far, we have used a constant ratio of specific heat capacities in our computations. In this subsection we wish to introduce γ as a variable property, thereby allowing for different specific heat capacities in the explosive products, relative to the surrounding atmosphere. Since RSPH is a particle method, this is easily obtained by introducing γ as a particle property. In the particle redistribution process of the simulation, we allow the particles to inherit γ in the same manner as for the other particle properties.

Table 2 Time correction relative to the empirical data at the first pressure sensor

Test	Type	Corrections (ms)
Spherical, HOB 1 m	RSPH	0.313
Spherical, HOB, 1 m	Chinook	0.365
Spherical, HOB, 2 m	RSPH	0.031
Cylindrical, HOB, 1 m	RSPH	0.051
$\gamma = \{1.3, 1.4\}$, HOB 1 m	RSPH	0.244

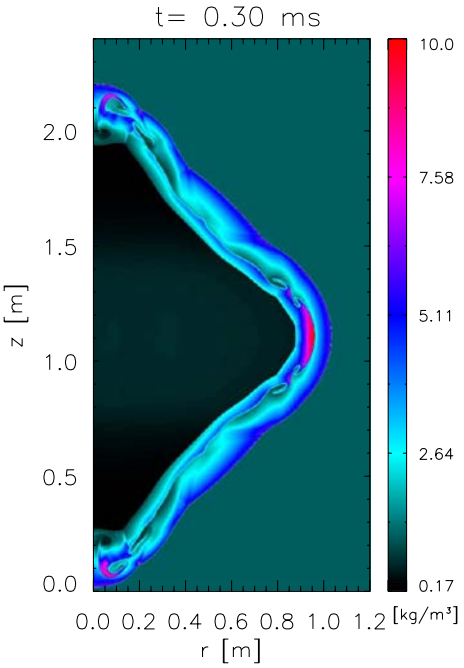

Fig. 7 Density color plot of a cylindrical charge, HOB = 1 m, at $t = 0.3$ ms after detonation initiation. The height is measured from the ground to the bottom of the charge

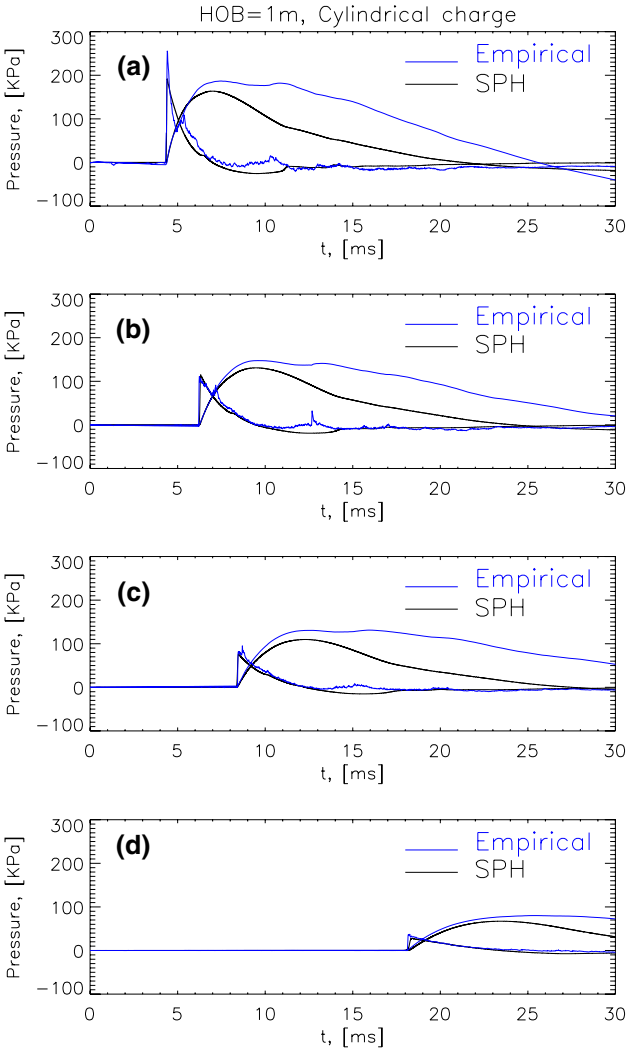

Fig. 8 Overpressure and pressure impulse plotted for a cylindrical charge at HOB = 1 m. Empirical results from pressure sensors (*black lines*) are compared to numerical results (*blue lines*). The pressure sensors are positioned at **a** $r = 4$, **b** 5, **c** 6 and **d** 10 m from ground zero

Our main goal with this study, is to investigate the effects of γ on the shock velocity, the pressure levels, and the position of the secondary shocks. The description will still be single phase, making use of the ideal gas equation of state. A parameter study on different γ values in the detonation products were performed choosing $\gamma = \{1.2, 1.25, 1.3, 1.35\}$. The spherical height of burst test, HOB = 1 m, was chosen as a test case. In the undisturbed atmosphere, we still have $\gamma = 1.4$ in all test cases.

Figure 9 illustrates the density and γ profile plotted for time, $t = 2$ ms, after detonation initiation. In this case, the explosive products in the dense balloon were assigned $\gamma = 1.3$. As time evolves the shock propagates outwards, and eventually reaches the ground, as illustrated in the density plot. The shock has now been reflected from the ground, and a complicated reflection pattern has formed. The right panel of Fig. 9 shows the γ profile at this stage, illustrating that only the innermost parts of the explosive products have the lower γ value.

The effect of reducing the ratio of specific heat capacities seems to be the generation of a faster propagating front shock, and consequently the smaller the γ value chosen is, the smaller is the correction value found. The front pressure levels are largely unaffected by changes in γ. We also notice that the choice of γ value seems to have little effect on the arrival of the small secondary shock. This result can be concluded from inspection of Fig. 10 and the right-hand panels of Fig. 6. In Fig. 10, we have plotted the empirical and numerical

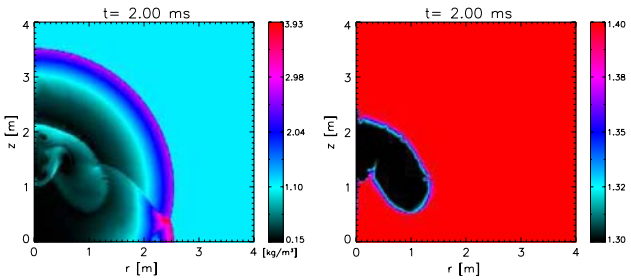

Fig. 9 Density (*left panel*) and γ (*right panel*) color plots for $t = 2$ ms after initiation

results for $\gamma = 1.3$. Comparing these figures, we observe that the position of the secondary shock is nearly unaffected by the choice of γ. As Table 2 illustrates, the time correction is found to be somewhat lower than in the constant $\gamma = 1.4$

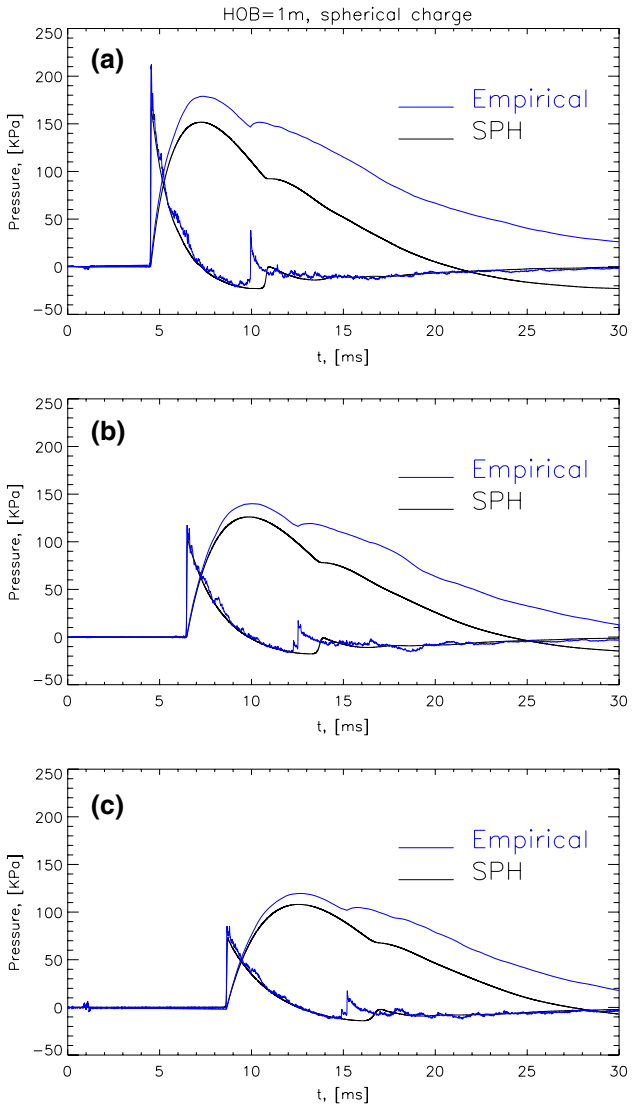

Fig. 10 Overpressure and pressure impulse plotted for empirical pressure recordings (*blue lines*) and numerical results (*black lines*). The explosive products were given $\gamma = 1.3$, whereas the surrounding atmosphere has a $\gamma = 1.4$. Sensors were positioned at distances of $d = 4$, 5, and 6 m

case. The pressure impulse for the $\gamma = 1.3$ case also seems to be unaffected by the choice of γ.

4.5 Triple point trajectories

In all the HOB test-cases presented, the shock is reflected from the ground as a regular reflection, but eventually develops into a Mach reflection. The Mach reflection is recognized by the fact that the reflection point leaves the surface, and that the incident shock, reflected shock and Mach stem coincide in one point called the triple point. This situation is illustrated in Fig. 9, left panel. We have used a series of density plots to determine the triple point trajectory for each of these

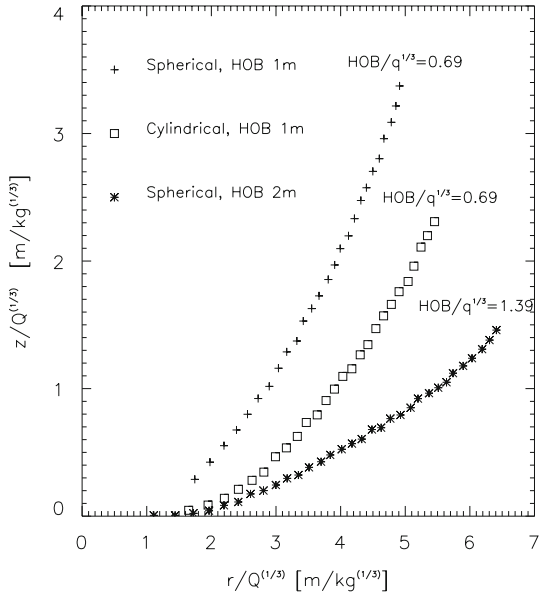

Fig. 11 Triple point trajectories for spherical and cylindrical charges. The trajectory is determined from the numerical density plots

tests. In Fig. 11, the results are presented for scaled distances [12] $r/Q^{1/3}$ and $z/Q^{1/3}$, where r, z, and Q are the distance along the ground, height above ground, and charge weight, respectively. The figure illustrates that for a spherical charge the steepest triple point trajectory is obtained for the lowest charge height. The effect of changing the shape of the charge to a cylindrical shape, with a $l/d = 2$, results in a flattening of the curve for the same charge height.

5 Summary and conclusions

In this paper we have used RSPH with our spherical and axisymmetric formulations together with the CVM to study blast wave propagation and reflection. When numerical and experimental results from free-field explosions are compared, the agreement is good for overpressure and time of arrival data. The positive phase duration and impulse results are less accurately described. The comparison between different empirical data, however, illustrates that there are considerable discrepancies in the empirical data for these quantities, indicating that these parameters are more difficult to measure accurately.

In the HOB test cases, pressure sensor recordings for different distances from the charge allow direct comparison between numerical and empirical results. In all three cases, we find the shock velocity and overpressure to be well captured by the numerical results. Pressure impulse and secondary features show some discrepancy between numerical and empirical results. The simulations with the commercial code, Chinook illustrate the same observed trends.

The introduction of the ratio of specific heat capacities as a particle property was done to study the effect of introducing a different values of γ for the explosive products. We find that changes in the γ values do not affect the overpressure level, but has an effect on the time of arrival of the shock. The smaller the γ chosen is, the smaller is the correction value needed. We also find that the choice of γ value has little effect on the arrival time of the secondary shock.

It should be mentioned that there are clearly challenges concerned with performing quantitative accurate experiments, and that factors such as the accurate position of detonator in the charge, homogeneous packing of the HE, the introduction of a wooden platform on which the charges were positioned, all are factors that may influence the results, and which are difficult to describe in a numerical code.

In the second HOB test, where the Chinook and RSPH codes are compared, we find good agreement between the two numerical results. In fact, when plotted in the same figure, the two numerical results are difficult to distinguish from each other. The two numerical methods differs in many aspects, Chinook being an Eulerian code and RSPH a Lagrangian method. RSPH has the advantage of allowing the particle distribution or resolution to be redefined at regular time intervals. This functionality is not available in Chinook. Since particles are used to the describe the dynamics of the system, it is relatively straight forward to include new particle properties, as demonstrated with the γ introduced as a particle property.

In this work, we have used the same explosive model, CVM in both numerical methods. The presented results show that the CVM adequately describes detonation of the HE TNT and C-4. The effect of afterburning has not been taken into account in the current study, but for some HE this may be an important effect, and consequently more advanced explosive models should be considered.

References

1. Baker, W.E.: Explosions in Air. University of Texas Press, Austin (1973)
2. Børve, S., Omang, M., Trulsen, J.: Regularized smoothed particle hydrodynamics: a new approach to simulating magnetohydrodynamic shocks. Astrophys. J. **561**, 82–93 (2001)
3. Børve, S., Omang, M., Trulsen, J.: Regularized smoothed particle hydrodynamics with improved multi-resolution handling. J. Comput. Phys. **208**(1), 345–367 (2005)
4. Dewey, J.M.: The air velocity in blast waves from tnt explosions. Proc. R. Soc. London **279**, 366–385 (1964)
5. Dewey, J.M., McMillin, D.J.: An analysis of the particle trajectory in spherical blast waves reflected from real and ideal surfaces. Can. J. Phys. **59**, 1380–1390 (1981)
6. Kingery, C.N., Bulmash, G.: Airblast parameters from spherical air burst and hemispherical surface burst. Tech. Rep. ARBRL-TR-02555, US Army Armament Research and Development Center (1984)
7. Kinney, G.F., Graham, K.J.: Explosive shocks in air, 2nd edn. Shock and Vibration. Springer, Berlin. ISBN-3-540-15147 (1985)
8. Monaghan, J.J.: Smoothed particle hydrodynamics. Rep. Prog. Phys. **68**(8), 1703–1759 (2005)
9. Omang, M., Børve, S., Trulsen, J.: Alternative kernel functions for smoothed particle hydrodynamics in cylindrical symmetry. Shock Waves **14**(4), 293–298 (2005)
10. Omang, M., Børve, S., Trulsen, J.: SPH in spherical and cylindrical coordinates. J. Comput. Phys. **213**(1), 391–412 (2006)
11. Omang, M., Børve, S., Trulsen, J.: Shock collisions in 3d using an axi-symmetric regularized smoothed particle hydrodynamics RSPH code. Shock Waves **16**, 467–475 (2007)
12. Sachs, R.G.: The dependence of blast on ambient pressure and temperature. Tech. Rep. BRL report No. 466, Aberdeen Proving Ground, Maryland (1944)
13. Settles, G.S., Keane, B.T., Anderson, B., Gatto, J.A.: Shock waves in aviation security and safety. Shock Waves **12**, 267–275 (2003)
14. Toro, E.F., Spruce, M., Spears, W.: Restoration of the contact surface in the HLL-riemann solver. Shock Wave **4**, 25–34 (1994)